

1 Performance of a passive acoustic 2 linear array in a tidal channel

3 Matthew F. Auvinen, David R. Barclay

4 **Abstract**

5 Baseline ambient sound level assessment is important in quantifying noise contributions from tidal energy
6 infrastructure. Static acoustic sensing in high-flow conditions is complicated by pseudo-sound, or flow noise,
7 generated by pressure fluctuations due to turbulent flow on the surface of a hydrophone. Signal processing methods
8 are used to identify and suppress flow noise at low frequencies (< 500 Hz) in data collected on a four element
9 horizontal hydrophone array in the Minas Passage, a tidal channel in the Bay of Fundy, in October 2016. Spectral
10 slope analysis is used to identify the spectral critical frequency, where the flow noise and ambient noise contributions
11 to the recorded signal are equal. Spatial coherence analysis is used to identify the coherence critical frequency, the
12 highest frequency at which flow noise can be detected. The array's performance in the Minas Passage is quantified
13 by an empirical relationship between flow speed and the spectral critical frequencies of the coherent output from
14 the liner array. Coherent averaging (broadside beamforming) is demonstrated as an effective flow noise suppression
15 technique, improving low-frequency passive acoustic monitoring in a high-energy tidal channel.

16 **Index Terms**

17 Flow noise, ambient noise, array processing, tidal channel, and passive acoustic monitoring.

18 **I. INTRODUCTION**

19 **T**IDAL power utilities are currently leasing seafloor space within the Minas Passage in the Bay
20 of Fundy with aspirations of converting the energy of the region's tidal currents into electricity,
21 a trend that has been supported by favorable projections of the Passage's tidal energy capacity [1]. As
22 these companies seek sector development, it is important that they maintain sustainable industry practices.

Dr. David Barclay is an assistant professor in the Department of Oceanography, Dalhousie University. Matthew Auvinen holds a B.Sc. (Hons) from the Department of Oceanography, Dalhousie University, Halifax, NS (email: matthewauvinen@gmail.com; dbarclay@dal.ca).

Manuscript received June 30, 2017; revised MONTTH XX, 201X. This work was supported by the Natural Sciences and Engineering Research Council of Canada, GeoSpectrum Technologies, and Black Rock Tidal Power.

23 This includes the consideration of industry knowledge gaps, many of which are a consequence of the
24 sector's immaturity [2]. The uncertainty surrounding the ecological and environmental implications of
25 tidal turbine infrastructure is a particularly important knowledge gap and has qualified some opposition
26 to turbine projects.

27 Tidal turbines present two serious environmental threats: physical contact (or interaction) with marine
28 life [3] [4] and acoustic pollution.

29 Tidal turbines could become an important source of ambient noise in tidal channels through cavitation
30 and motor or mechanical noise [5]. Turbine anthropophony could affect animal navigation, communication,
31 predator-prey detections [6], and marine life cycles [7]. Moreover, turbine-generated sound could be
32 damaging to fish tissue [8]. If substantive, these effects would threaten near-field and far-field ecosystem
33 health, stressing the need for rigorous environmental impact assessments in the tidal power sector.

34 As a result, stakeholders, regulators, and tidal power companies are interested in establishing baseline
35 ambient noise measurements in the Minas Passage, against which turbine noise pollution will be measured.
36 However, the utility of ambient sensing is limited by pseudo-sound, or flow noise, generated on the surface
37 of a hydrophone in turbulent water. Indeed, the masking effects of flow noise can complicate source
38 identification and background noise assessment in high-flow settings, such as tidal channels.

39 Analogous to turbulent flowing air [9], flowing water in a high Reynolds number regime generates
40 pressure fluctuations on the surface of a hydrophone. These pressure fluctuations produce flow noise
41 which is irregular, uncorrelated, and random. Local pressure fluctuations on the surface of a hydrophone
42 represent near-field turbulence [10]. Free-drifting hydrophones moving with the mean water flow will
43 experience little signal contamination, as it is the relative flow of water over a hydrophone's surface that
44 leads to flow noise.

45 Turbulent flows occupy a wide range of frequencies and wavenumber domains, with broad spatial and
46 temporal variability. The advective nonlinearity of turbulent flows makes them unpredictable in space and
47 time, and contributes to their complex nature [11]. As such, it is difficult to reliably model flow noise.

48 Flow noise follows a spectral slope of $f^{-5/3}$ at low frequencies, behaviour that is analogous by
49 Kolmogorov's turbulence theory. This flow noise is not to be confused with wind-generated noise that
50 produces $f^{-5/3}$ spectral slopes at higher frequencies [12]. Bassett et al. [13] identifies $f^{-5/3}$ flow noise
51 below 20 Hz and also describes steepened spectral slopes, f^{-m} , at low-to-mid frequencies. Lombardi [6]
52 identifies these steep spectral slopes in measurements from the Grand Passage tidal channel. The flow

53 noise that produces f^{-m} is a result of small-scale turbulence being averaged out across the surface of the
54 hydrophones, which dampens (or reduces) measurements.

55 Flow noise presents a unique challenge for passive acoustic monitoring (PAM): a hydrophone in a
56 high-flow setting will record both propagating sound and pseudo-sound. This suggests that models should
57 distinguish between the two sound sources. Barclay and Buckingham [14] describe the exploitation of
58 uncorrelated flow noise to identify pseudo-sound in deep ocean ambient noise measurements.

59 Successful suppression of flow noise could benefit PAM systems in the tidal energy sector. The objectives
60 of the present research are:

- 61 1) Use spectral analysis and spatial coherence to identify and characterize flow noise at low frequencies
62 (< 500 Hz).
- 63 2) Use coherent averaging (beamforming) to improve the performance of a linear hydrophone array
64 by suppressing flow noise and enhancing the measurement of ambient noise.

65 This paper is organized as follows. Section II discusses important field work details, including an
66 experiment description and instrumentation summary. Section III describes all relevant signal processing,
67 with emphasis on spectral analysis, spatial coherence, and beamforming. Section IV presents the signal
68 processing and data analysis results. Section V evaluates the results and identifies areas for future work.
69 Lastly, Section VI summarizes the findings of the study in a series of conclusions.

70 II. FIELD WORK

71 Field work was completed on October 27, 2016, near the Fundy Ocean Research Center for Energy
72 (FORCE) site in the Minas Passage of the Bay of Fundy. The deployment period spanned roughly four
73 hours, from 12:00 ADT to 16:00 ADT. This experimental window captured the transition from ebb tide
74 to slack tide.

75 Wind speed was measured intermittently throughout the deployment period using a hand-held wind
76 speed gauge. Tidal and flow data was generated using a WebTide model [15].

77 A. Experiment

78 A linear hydrophone array was streamed behind the *MV Nova Endeavour* (42' x 16'), which was
79 anchored to the seafloor in the Minas Passage. The array was positioned 15 meters below the sea surface
80 using a depressor. Four hydrophones were simultaneously sampled over a four hour period and processed

81 by an analog-to-digital converter (ADC) on board the *MV Nova Endeavour*. The signal cable, which
 82 carried both the array and a drogue, was sheathed in a fairing to reduce strum generation and attached to
 83 a tow cable (6GA galvanized wire) using cable ties.

84 A drifting hydrophone (Geospectrum Technologies GuardBuoy) was deployed using a small auxiliary
 85 vessel launched from the *MV Nova Endeavour*. The GuardBuoy was suspended 2 meters below the surface
 86 using a drifting surface float and isolation system made of non-stretch line and compliant bungee. The
 87 system isolated the recording hydrophone and instrument package from any surface action, such as the
 88 vertical movement of waves, which would otherwise generate mechanical or flow noise.

89 A total of five transects were performed by driving the GuardBuoy upstream, deploying the drifter,
 90 then floating downstream in a rigid-hulled inflatable boat (RHIB) a modest distance from the GuardBuoy.
 91 The GuardBuoy and RHIB followed a downstream transect that passed over the array. The GuardBuoy
 92 was retrieved once it had reached 20 meters beyond the array. These transects were performed over the
 93 course of three hours, beginning at 13:00 ADT. The GuardBuoy signals are assumed to be free of flow
 94 noise and were used as benchmarks to assess the performance of the array. The turbulent tidal channel
 95 is assumed to be well mixed with an isovelocity sound speed profile, minimizing noise field variability
 96 over the depth difference between the two systems.

97 *B. Instrumentation*

98 The linear array was constructed by GeoSpectrum Technologies, and contains four sequentially spaced
 99 hydrophones with a horizontal configuration. Each neighbouring hydrophone is separated by a distance
 100 $d = 17\text{cm}$. The array hydrophones were set to simultaneously sample at a rate of 96.038 kHz with an
 101 acoustic bandwidth of 48.019 kHz. The four channels on the array continuously recorded 10 minute WAV
 102 files over a 4 hour period. Power spectra were calibrated to dB re $1 \mu\text{Pa}$ according to frequency-dependent
 103 sensitivities supplied by the manufacturer. The GuardBuoy sampled at a rate of 96 kHz with an acoustic
 104 bandwidth of 48 kHz, and was equipped with a GPS to record transect geospatial information. The Guard
 105 Buoy recorded WAV files in 30 minute segments. Corresponding power spectra were converted to dB re
 106 $1 \mu\text{Pa}$ according to frequency-dependent sensitivities supplied by the manufacturer.

107 III. DATA ANALYSIS

108 Data analysis was performed in MATLAB in several stages. The analysis began with the calculation of
 109 the power spectral density (PSD) from the raw WAV files, followed by spectral analysis, spatial coherence

¹¹⁰ analysis, and broadside beamforming.

¹¹¹ *A. General Signal Processing*

The output of a hydrophone is defined as

$$x_i(t) = \sigma_i(t) + n_i(t) \quad (1)$$

¹¹² where x_i is the recorded time series on each i th hydrophone, σ_i is the sound field's ambient components,
¹¹³ and n_i is the locally generated flow noise. Importantly, n_i and σ_i are uncorrelated. Furthermore, the
¹¹⁴ inherent randomness of flow noise makes n_i incoherent with respect to n_j .

The power spectrum, or spectral density, is defined as

$$S_{ii}(\omega) = \frac{\langle X_i(\omega) \cdot X_i^*(\omega) \rangle}{T} \quad (2)$$

¹¹⁵ where X_i is the Fourier transform of x_i , ω is angular frequency, $*$ denotes a complex conjugate, $\langle \rangle$
¹¹⁶ indicates an ensemble average, and T is the observation interval. All Fourier transforms are windowed
¹¹⁷ by a Hann function. The Fourier transform is 2^{16} points long and contains 99 degrees of freedom.

Coherence is used to quantify the similarity between two signals and is defined as

$$\Gamma_{ij}(\omega) = \frac{S_{ij}(\omega)}{(S_{ii}(\omega) \cdot S_{jj}(\omega))^{\frac{1}{2}}}. \quad (3)$$

¹¹⁸ *B. Power Spectrum Probability Density*

¹¹⁹ Spectral probability density (SPD) is an analytical technique used to depict the variability of the power
¹²⁰ spectrum over a period that is much longer than the minimum time required for a stationary measurement
¹²¹ of power to be made [16]. This form of analysis facilitates the identification of unique events within a
¹²² series of spectra.

The power spectrum probability density (PSPD) is defined as

$$\text{PSPD}(f) = H(S_{ii}(f), h) \quad (4)$$

¹²³ where $\text{PSPD}(f)$ is the power spectrum probability density at frequency f , and $H(S(f), h)$ is the histogram
¹²⁴ of the power spectrum S_{ii} at frequency f with a histogram bin width of h dB re 1 μPa . By combining

¹²⁵ PSPD results across frequencies, we generate a PSPD matrix

$$\begin{bmatrix} \text{PSPD}(f_1) & \text{PSPD}(f_2) & \text{PSPD}(f_3) & \dots & \text{PSPD}(f_a) \end{bmatrix} \quad (5)$$

¹²⁶ where $\text{PSPD}(f_a)$ is the PSPD at the a th frequency.

¹²⁷ *C. Spectral Critical Frequency*

¹²⁸ Lombardi [6] and Bassett et al. [13] suggest that there are three distinct spectral slope regions in
¹²⁹ the low-to-mid-frequency range: spectral slopes of Kolmogorov's $f^{-5/3}$; steepened flow noise spectral
¹³⁰ slopes, f^{-m} , that include the effects of a finite volumed sensor [13]; and an ambient noise region that is
¹³¹ determined by near-field and far-field ambient sound sources.

The local spectral slope is defined as

$$f^{-M} = \frac{S_{ii}(2\pi f_a) - S_{ii}(2\pi f_b)}{\log(f_a \cdot f_b^{-1})} \quad (6)$$

¹³² where $S_{ii}(2\pi f_a)$ is the spectral density on the i th sensor at frequency f_a and $S_{ii}(2\pi f_b)$ is the spectral
¹³³ density on the i th sensor at frequency f_b . (6) describes the spectral slope in dB/decade.

The transition from the flow noise region of f^{-m} to the ambient noise region is marked by the frequency knee, where the spectral slope begins to shallow. That is, the exit from the flow noise region is marked by a deviation below the slope f^{-m} . Here, the spectral critical frequency, f_c , is defined as the first frequency at which

$$|f^{-M}| < |f^{-m}| \quad (7)$$

¹³⁴ is true. Importantly, both slopes in (7) are in dB/decade.

¹³⁵ *D. Coherence Critical Frequency*

¹³⁶ Spatial coherence is calculated for each channel combination using (3), providing an assessment of
¹³⁷ signal similarity between elements. Propagating ambient noise is highly correlated across the array.
¹³⁸ Additionally, propagating noise at wavelengths sufficiently large relative to element spacing produces
¹³⁹ very high coherence at low frequencies by effectively co-locating sensors. Conversely, flow noise is a
¹⁴⁰ source of incoherence, as pseudo-sound is uncorrelated across the linear array (when turbulent scales are
¹⁴¹ lesser than hydrophone separation). Therefore, in the band $f < 500$ Hz, flow noise is marked by low

142 coherence while ambient noise is marked by high coherence. The transit of this coherence boundary, from
 143 flow noise (incoherent) to ambient noise (coherent) provides a metric for describing the extent of flow
 144 noise across the array.

The coherence critical frequency, f'_c , is defined as the frequency at which a minimum coherence threshold is crossed due to flow noise masking. To establish this coherence threshold, we assume an isotropic ambient noise field such that the horizontal coherence is given by Buckingham [17]

$$G_{ij}(\omega') = \frac{\sin(\omega'_{ij})}{\omega'_{ij}} \quad (8)$$

where

$$\omega'_{ij} = \frac{2\pi d_{ij} f}{c}. \quad (9)$$

Here, d_{ij} is the separation distance between the i th and j th hydrophone and c is the local sound speed. We define f'_c as the first frequency at which

$$|\Gamma_{ij}(\omega')| \geq 0.9 \cdot G_{ij}(\omega') \quad (10)$$

145 is true. We can be confident that any coherence within 10% of (8) is real and significant while any
 146 drop below the threshold given by the right hand side of (10) is caused by the addition of flow-generated
 147 incoherent noise. This automated critical frequency detector corresponds to a coherence threshold of ~ 0.9 .
 148 The use of a more sophisticated noise model such as Cron and Sherman [18] or Deane and Buckingham
 149 [19] in the place of (8) yields a nearly identical threshold.

150 E. Linear Regression

151 Linear regressions between critical frequencies, f_c and f'_c , and flow speed, u , are used to identify and
 152 characterize the prevalence of flow noise and ambient noise in measurements. No data points are excluded
 153 from these regression.

154 F. Beamforming

We use a broadside beamformer to coherently average the channels across the array. Locally generated flow noise and the ambient sound field are inseparable, however we can describe their relative prevalence

with the theoretical signal-noise ratio (SNR) where we are defining ambient sound as the signal, and flow noise as the noise. By taking the Fourier transform of (1) and substituting into (2), we find

$$S_{ii} = \frac{\langle (\varsigma_i + N_i) \cdot (\varsigma_i^* + N_i^*) \rangle}{T} \quad (11)$$

where ς_i and N_i are the Fourier transforms of σ_i and n_i , respectively. For clarity, the frequency dependency has been omitted. Since ς_i and N_i are uncorrelated, we can expand (11) to arrive at

$$S_{ii} = \frac{\langle \varsigma_i \varsigma_i^* \rangle + \langle N_i N_i^* \rangle}{T}. \quad (12)$$

Given (12), the SNR for a single hydrophone (SNR_H) is defined as

$$\text{SNR}_H = \frac{\langle \varsigma_i \varsigma_i^* \rangle}{\langle N_i N_i^* \rangle} \quad (13)$$

where $\text{SNR}_H = 1$ at the critical frequency, f_c . Now consider an array of hydrophones indexed by i , where the ambient sound field component of the signal on each phone is

$$\sigma_{i+1}(t) = \sigma_1(t - \tau_i) \quad (i > 1) \quad (14)$$

where

$$\tau_i = \frac{i \cdot d \cos \theta}{c} \quad (15)$$

is the acoustic travel time in seconds for plane wave noise arriving on the sensors at the angle θ . Here, d is the nearest neighbour element separation. Taking the Fourier transform of (14) gives

$$\varsigma_i(\omega) = \varsigma_1(\omega) e^{-i\omega\tau_i}. \quad (16)$$

The coherent sum of the signals across the array is defined as

$$x_T(t) = \sum_{i=1}^l x_i(t) \quad (17)$$

where $x_i(t)$ is the signal recorded on the i th element of a linear array l elements long. Since no time delay has been applied to $x_i(t)$, $x_T(t)$ is the equivalent to beamforming broadside to the array. Since the source of interest is ambient noise, the sound field is assumed to be axially symmetric. Thus the horizontal array orientation and beam direction are unimportant, provided an appropriate array gain compensation

is applied. The Fourier transform of (17) is

$$X_T(\omega) = \sum_{i=1}^l X_i(\omega). \quad (18)$$

The array power spectral density can be estimated using (18) by

$$A = \frac{\langle X_T(\omega) \cdot X_T^*(\omega) \rangle}{T}. \quad (19)$$

Given an array with both ambient noise and flow noise components, (18) can be expanded to

$$X_T = [\varsigma_1 + N_1 + \varsigma_2 + N_2 + \dots + \varsigma_l + N_l] \quad (20)$$

which describes the total output of all sensors on an array with l elements. Substituting (16) into (20) gives

$$X_T = \varsigma_1 + N_1 + \sum_{i=1}^l (\varsigma_1 e^{-i\omega\tau_i} + N_{i+1}). \quad (21)$$

Using the Fourier transform of the coherently summed outputs across the array, the power spectral density can be computed by substituting (21) into (19) yielding

$$A = \frac{\langle \varsigma_1 \varsigma_1^* \left[l + \sum_{i=1}^{l-1} \frac{1}{2} (l-i) \cos(\omega\tau_i) \right] + N \cdot N^* \rangle}{T} \quad (22)$$

where

$$N = \sum_i^l N_i \quad (23)$$

is the coherently summed flow noise. This term can be simplified by assuming the power of the flow noise measured on each individual hydrophone is equal across the array,

$$\langle N_i N_i^* \rangle = \langle N_j N_j^* \rangle \quad (24)$$

and uncorrelated between the sensors,

$$\langle N_i N_j^* \rangle = \delta_{ij} \cdot N_1 N_1^* \quad (25)$$

155

$$\delta_{ij} = \begin{cases} 0 & \text{if } i \neq j \\ 1 & \text{if } i = j. \end{cases}$$

Then the total power received by the array becomes

$$A = \frac{\langle \varsigma_1 \varsigma_1^* \rangle \left[l + \sum_{i=1}^{l-1} \frac{1}{2} (l-i) \cos(\omega \tau_i) \right] + l \langle N_1 N_1^* \rangle}{T}. \quad (26)$$

Furthermore, if K is defined as

$$K = l + \sum_{i=1}^{l-1} \frac{1}{2} (l-i) \cos(\omega \tau_i) \quad (27)$$

then (26) becomes

$$A = \frac{K \langle \varsigma_1 \varsigma_1^* \rangle + l \langle N_1 N_1^* \rangle}{T} \quad (28)$$

where (28) describes the array spectral density. Here, SNR_A describes the relative strength of the ambient noise and flow noise components of the array output, such that

$$SNR_A = \frac{K \langle \varsigma_1 \varsigma_1^* \rangle}{l \langle N_1 N_1^* \rangle}. \quad (29)$$

156 Comparing (29) to the result derived for a single hydrophone, given by (13), we see that the beamformed
 157 array improves the signal-to-noise ratio by a factor of $\frac{K}{l}$. Furthermore, (29) suggests that array performance
 158 improves with an increasing number of hydrophones, l . For an array with 4 elements, at broadside, $\frac{K}{l} =$
 159 $\frac{7}{4}$.

160 *G. Array Gain*

The broadside beamforming analysis applied to the linear array generates artificial spectral density gain. As a result, an array gain formula is applied to the beamformed results to correct the inflated values. The array gain formula presented here is adapted from Cox [20], such that

$$AG = 20 \log l. \quad (30)$$

161 The array gain correction is performed by subtracting the result of (30) from the calculated array power
 162 spectral density.

163 *H. Algorithm Assessment*

164 (18) and (19) are used to consolidate all channel signals into one coherent array output. The coherent
 165 array spectral critical frequencies are compared to the spectral critical frequencies of a fixed single
 166 hydrophone to critically evaluate the performance of the beamformed array. GuardBuoy, fixed single
 167 hydrophone, and coherent array signals are compared to further assess the coherent array's performance.

168 IV. RESULTS

169 *A. Spectral Density*

170 Signal levels (Fig. 1) are relatively high in fast flowing water and low in slow flowing water. The
 171 mid-to-high-frequency band is less affected by flow noise and is quiet relative to lower frequencies (<
 172 10 Hz). Evidently, flow noise is prevalent below 100 Hz.

173 The wind speed varied between 3.2 and 6.2 m/s with a mean of 5.0 m/s. The hydrophone power
 174 spectrum contains multiple episodes of mid-frequency noise. These signals are attributed to ship noise
 175 generated by the small vessel used in the GuardBuoy drifter tests. Additionally, the abrupt shift in spectral
 176 density at 90 minutes is due to equipment reconfigurations.

177 *B. Power Spectrum Probability Density*

178 The PSPD facilitates the broad-scale assessment of a hydrophone's spectral density over entire deploy-
 179 ment periods. The PSPD for channel 0 is shown in Fig. 2.

180 The PSPD follows a spectral slope of $f^{-5/3}$ below 10 Hz, behaviour analogous to Kolmogorov's
 181 turbulence theory. This spectral slope marks a region of flow noise within the signal. A steepened spectral
 182 slope of f^{-m} , where $m > \frac{5}{3}$, persists between 10 and 100 Hz, a result of small-scale turbulence when
 183 turbulence wavelength \ll sensor size. This small-scale turbulence is averaged out over the surface of
 184 the hydrophone sensor, dampening the measured signals. The PSPD results show that ambient noise is
 185 dominant above 300 Hz, where signal levels are markedly low. Early in the deployment (around 10
 186 minutes) electronic noise in the system raised the noise floor to 90 dB μPa . While this was quickly
 187 remedied on site, an electronic system noise floor persisted at about 60 dB re μPa .

188 Single power spectra are superimposed on the PSPD and suggest that measurements in slow current
 189 conditions contain a greater extent of ambient noise relative to those in fast current conditions.

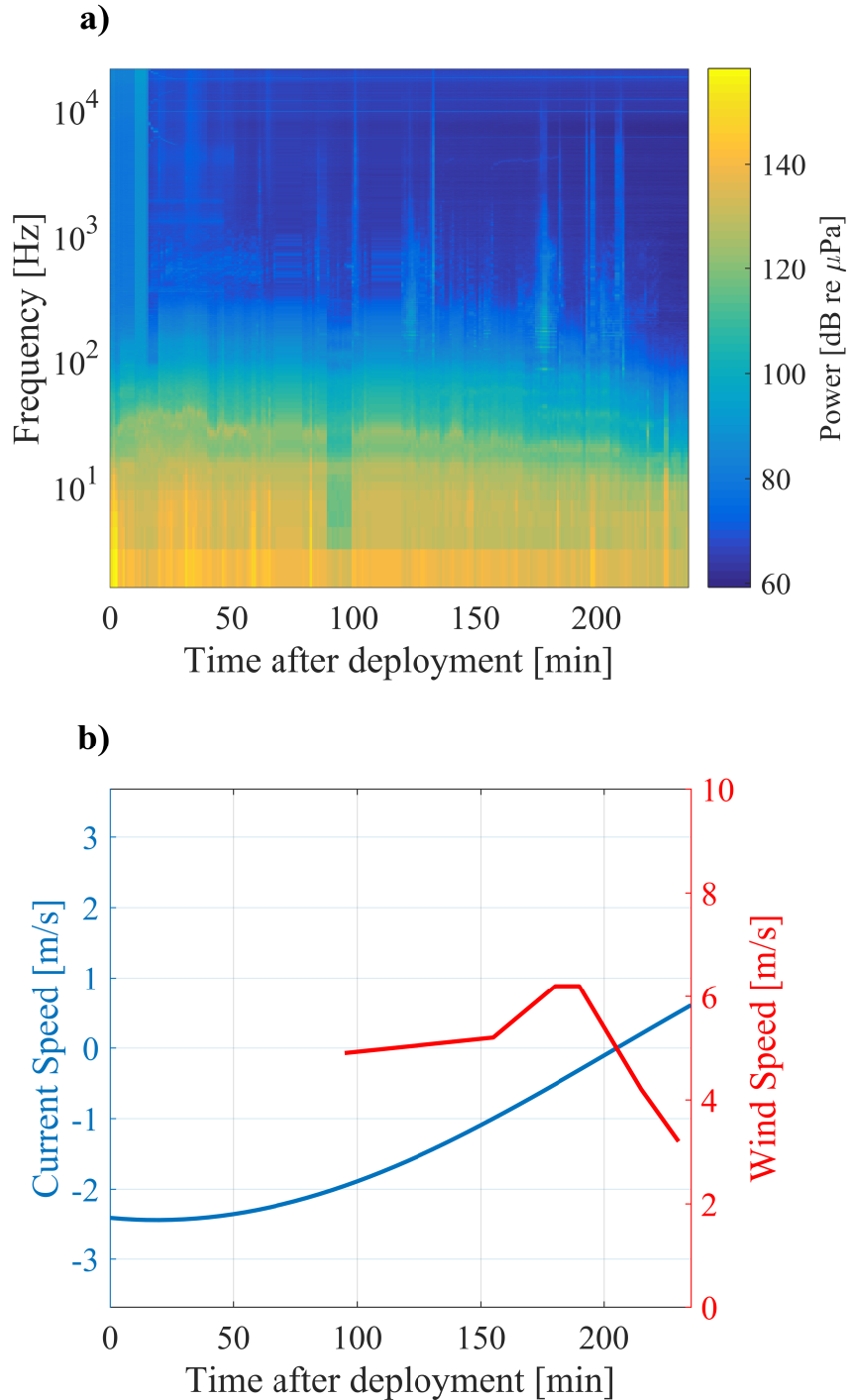


Fig. 1. Power spectrum for channel 0 on the array (a). The spectrum is plotted over the deployment period across a range of low-to-mid frequencies. The spectrum begins at maximum ebb tide and ends shortly after slack tide, as shown by the current speed time series (b). Power decreases with current speed over the deployment period.

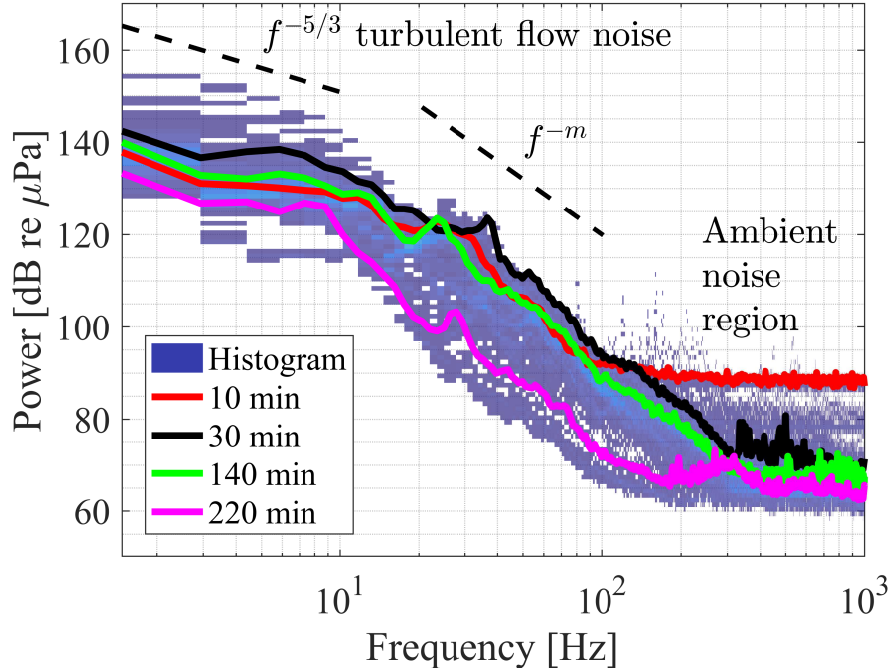


Fig. 2. Channel 0 power spectrum probability density over the entire deployment period. Turbulent flow noise is prevalent < 10 Hz (where wavelengths \gg sensor size), with a spectral slope of $f^{-5/3}$, while turbulence interacting with the hydrophone's finite volume (in the 10 Hz to 100 Hz band) yields a spectral slope of f^{-m} . The ambient sound field dominates at frequencies > 300 Hz. Coloured lines represent individual spectra recorded at the time after deployment indicated in the legend.

190 C. Spectral Critical Frequency

191 Spectral slopes were iteratively calculated between 10 and 100 Hz using (6). The linear relationship
 192 between spectral slope, f^{-m} , and current speed, u , (Fig. 3) indicates that signals recorded in decreasing
 193 flow are increasingly damped (steepened slope). The inverse relationship between current speed and
 194 spectral slope suggests that signals are less damped in fast flowing water, a result of larger turbulence
 195 scales. The spectral slopes observed between 10 and 100 Hz range from -25 to -60 dB/decade. The
 196 correlation coefficient, R , indicates that there is a meaningful correlation between spectral slope and
 197 current.

198 The spectral critical frequency was iteratively calculated over the experimental period using (7). These
 199 critical frequencies were regressed against current speed, as shown in Fig. 4. There is a positive correlation
 200 between spectral critical frequency and current speed, where fast flow coincides with high spectral critical
 201 frequencies. The spectral critical frequency is the frequency at which flow noise and ambient noise are
 202 equal in power.

203 The intercepts have not been forced to zero. This is because it is unrealistic to expect that we can com-
 204 pletely eliminate flow noise, or low-frequency noise generated by the mechanical systems that comprise

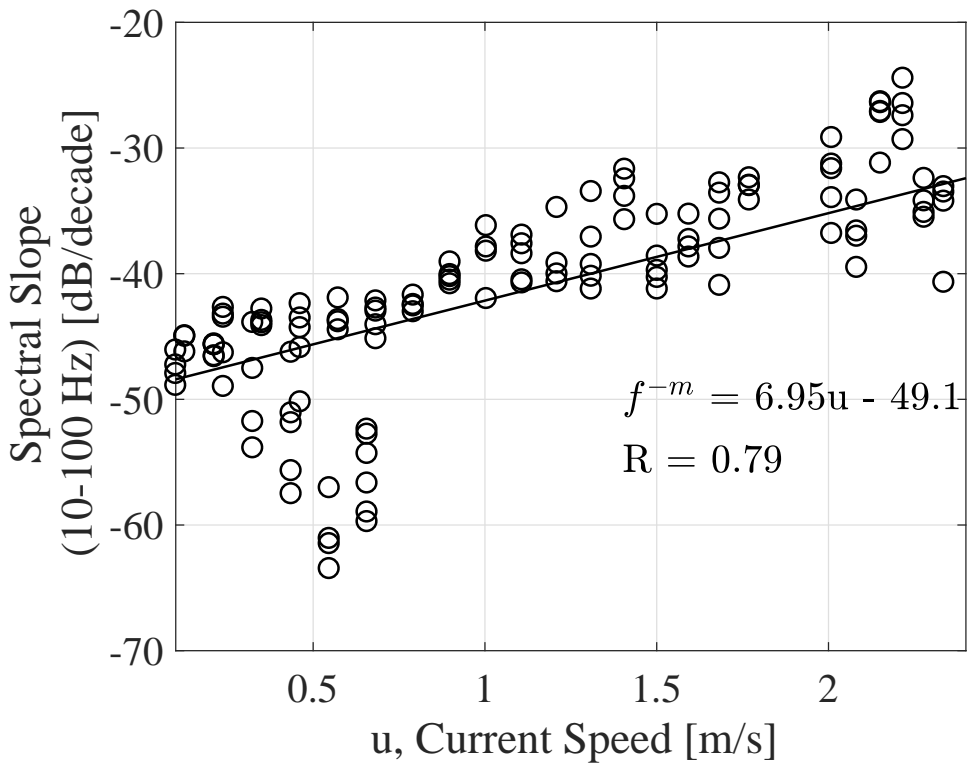


Fig. 3. Relationship between spectral slope, f^{-m} , and current speed, u , between 10 and 100 Hz for channel 0. Spectral slope magnitude increases with decreasing flow. The correlation coefficient, R , is reported.

205 the tow body. If this were a moored system with no surface expression, that assumption might be valid,
206 but is not considered here.

207 *D. Spatial Coherence*

208 Spatial coherence is calculated for different hydrophone combinations across the linear array using
209 (3). The spatial coherence results are presented in magnitude coherence for the entire deployment period
210 (Fig. 5). If the wavelength of propagating sound is sufficiently long (frequency sufficiently low) the
211 sensors would become relatively co-located and the coherence would tend to unity. However, the results
212 suggest that the low frequency data is overwhelmingly incoherent, since the locally generated flow noise
213 is incoherent from one hydrophone to the next.

214 Flow noise is uncorrelated and propagating ambient noise is highly correlated at low frequencies. As
215 a result, low coherence and high coherence are a sign of flow noise and ambient noise, respectively.
216 Therefore, the spatial coherence results are partitioned into two distinct regions: a flow noise region
217 and an ambient noise region. Visual assessment suggests that flow noise is consistently present at low
218 frequencies and can be prominent at higher frequencies (above 600 Hz). The ambient noise region is

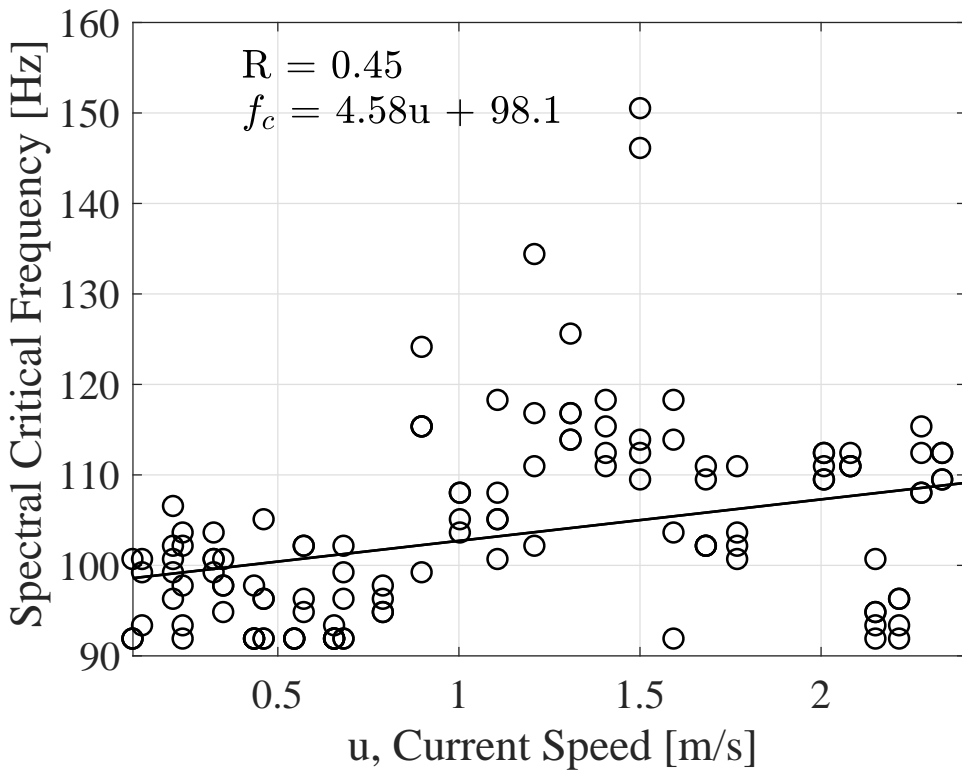


Fig. 4. Relationship between spectral critical frequency, f_c , and current speed, u , for channel 0. Spectral critical frequency marks where the flow noise and ambient noise contributions to the recorded signal are equal, and increases with current speed. Correlation coefficients, R , are reported.

present between 200 and 600 Hz and contains the same vessel noise identified in Fig. 2.

220 E. Coherence Critical Frequency

221 The coherence critical frequency is the highest frequency at which flow noise can be detected. The
 222 coherence critical frequency was iteratively calculated for each combination of channels, and is used to
 223 quantify the relative prevalence of flow noise and ambient noise within a measurement (Fig. 6). The
 224 coherence critical frequency is a more sensitive method of flow noise measurement than the spectral
 225 critical frequency, as spatial coherence is used as an indicator of flow noise cessation rather than relative
 226 noise contributions. The coherence critical frequency increases with increasing flow speed, a relationship
 227 similar to that of the spectral critical frequency.

228 It is important to note that the coherence is impacted by any temporary deterministic noises present in
 229 the sound field, such as the auxiliary RHIB, mechanical array noise, or noise generated aboard the *MV*
 230 *Nova Endeavour*. In such instances, the automated coherence critical frequency detector fails, and yields
 231 an outlier.

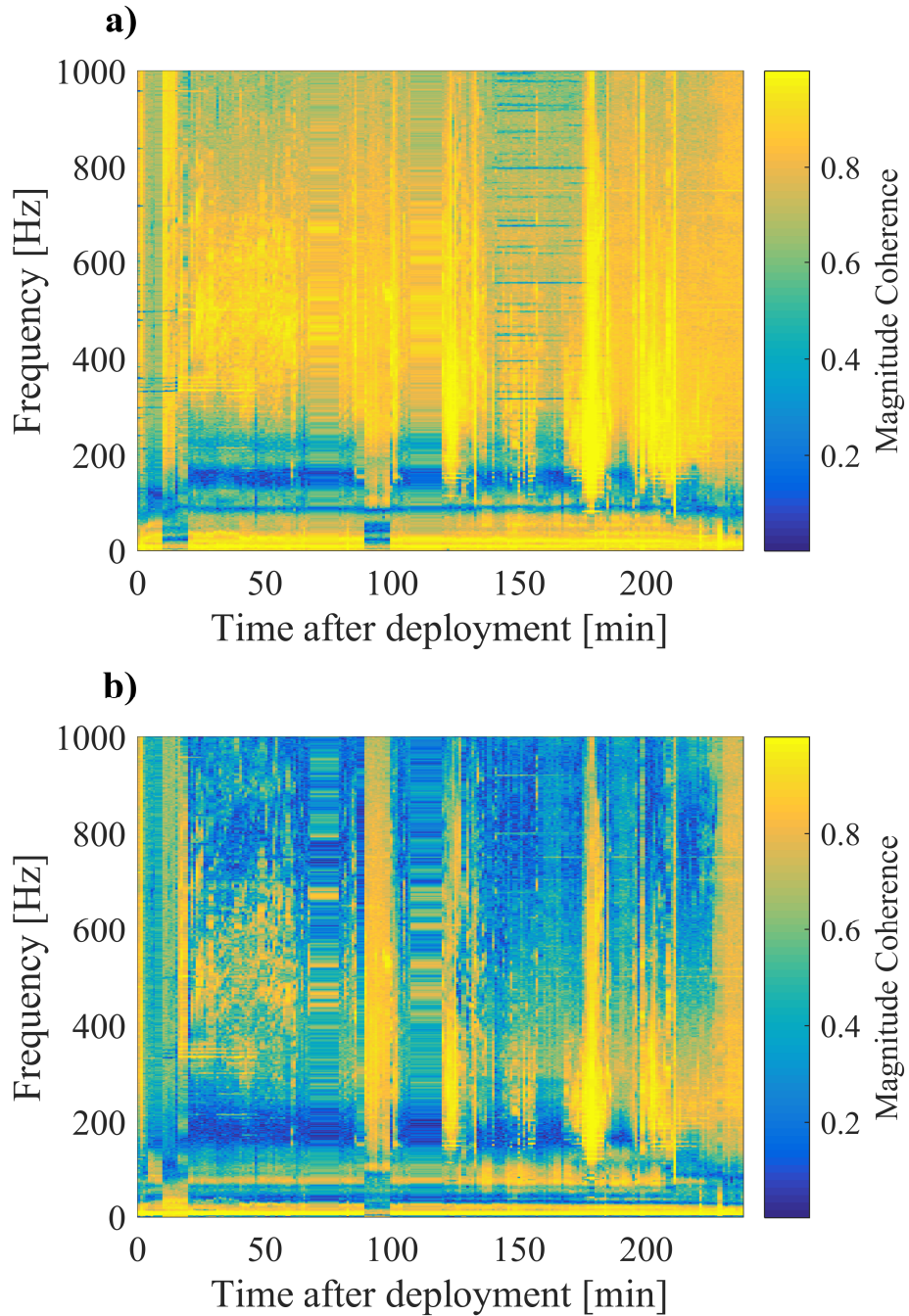


Fig. 5. Spatial coherence over the experimental period. Magnitude coherence is expected to tend to unity as the fixed hydrophones become relatively co-located. However, uncorrelated flow noise on each phone breaks that relationship. The extent of incoherent flow noise increases with current speed. Channel 0 - 1 (a) and 0 - 3 (b) are shown as examples. Results hold to all other channel combinations.

232 There is a good deal of noise in Fig. 6, as no outliers nor oddities were discarded. The retention of
 233 outliers is done to maintain the integrity of the linear regression and the correlation present.

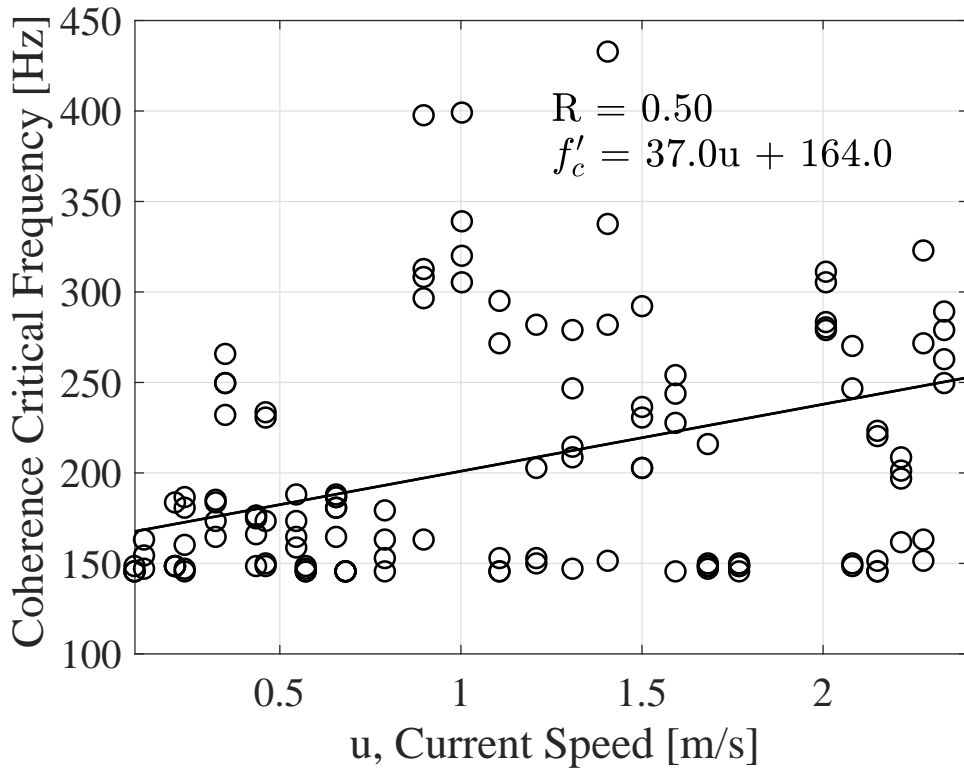


Fig. 6. Relationship between coherence critical frequency, f'_c , and current speed, u , for channels 0 - 1. Coherence critical frequency is the highest frequency at which flow noise can be detected, and increases with current speed.

234 F. Beamforming

235 The spectral critical frequency of the coherent array output is compared to the fixed single hydrophone
 236 spectral and coherence critical frequencies in Fig. 7. The standard deviations of the spectral slope and
 237 spatial coherence critical frequency regressions were extracted from the averaged fits, while the standard
 238 deviation of the coherent array critical frequency regression was calculated from the data during the
 239 regression.

240 The coherence critical frequencies are relatively high, while spectral critical frequencies (both fixed
 241 single hydrophone and coherent array) are relatively low. This is attributed to the more sensitive nature
 242 of the coherence-based method. Above coherence critical frequencies we can be confident that there is
 243 no contamination of the ambient noise field by flow noise. Conversely, the fixed single hydrophone and
 244 coherent array spectral critical frequencies show where flow noise and ambient noise have equal power.
 245 The coherence and spectral critical frequencies serve as the respective upper and lower bounds of different
 246 noise regimes. Importantly, the coherent array output contains significantly lower critical frequencies than
 247 the fixed single hydrophone, indicating that the broadside beamforming approach lessens the extent of

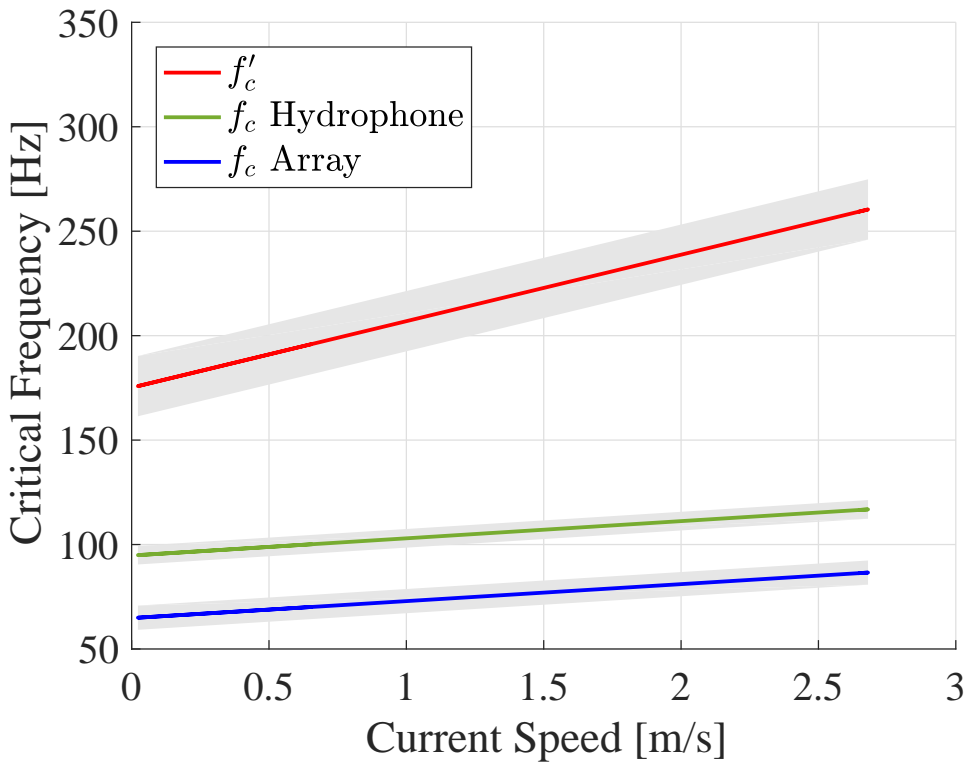


Fig. 7. Comparison of fixed single hydrophone spectral critical frequency (green), coherence critical frequency (red), and array spectral critical frequency (blue) distributions. Uncertainties are one standard deviation (shaded). Coherence critical frequency, f'_c , serves as the upper frequency bound, above which flow noise is negligible. Spectral critical frequency, f_c , serves as the lower frequency bound, below which flow noise is greater than ambient noise. Between these two bounds the signal is comprised of both flow noise and ambient noise. The coherent array effectively suppresses flow noise, as indicated by its improved lower frequency bound relative to the fixed single hydrophone.

248 flow noise within the measurements.

249 Fig. 8 compares GuardBuoy, fixed single hydrophone, and horizontal coherent array power spectra at
250 1.5 hours into the experiment. We select a time where the drifter and array were in close proximity to
251 establish a meaningful comparison.

252 The GuardBuoy spectrum behaves differently from the rest, exhibiting lower levels at frequencies
253 below 100 Hz. A pronounced excursion in spectral slope is present at 10 Hz in the GuardBuoy spectrum,
254 suggesting non-negligible flow noise is affecting the drifter's low-frequency measurements. This is typical
255 of all moored or free drifting passive acoustic systems that have a surface expression or subsurface float.
256 The fixed single hydrophone shows clear symptoms of flow noise at low frequencies.

257 The spectra reveal that the coherent array spectra transitions to the ambient noise region at lower
258 frequencies than the fixed single hydrophone. Furthermore, the coherent array signals are quieter than
259 the fixed single hydrophone signals at all low frequencies, demonstrating the effective suppression of
260 flow noise. There is reasonable agreement between the GuardBuoy and coherent array above the critical
261 frequency, with some difference above 700 Hz. This disparity is attributed to the lack of co-location

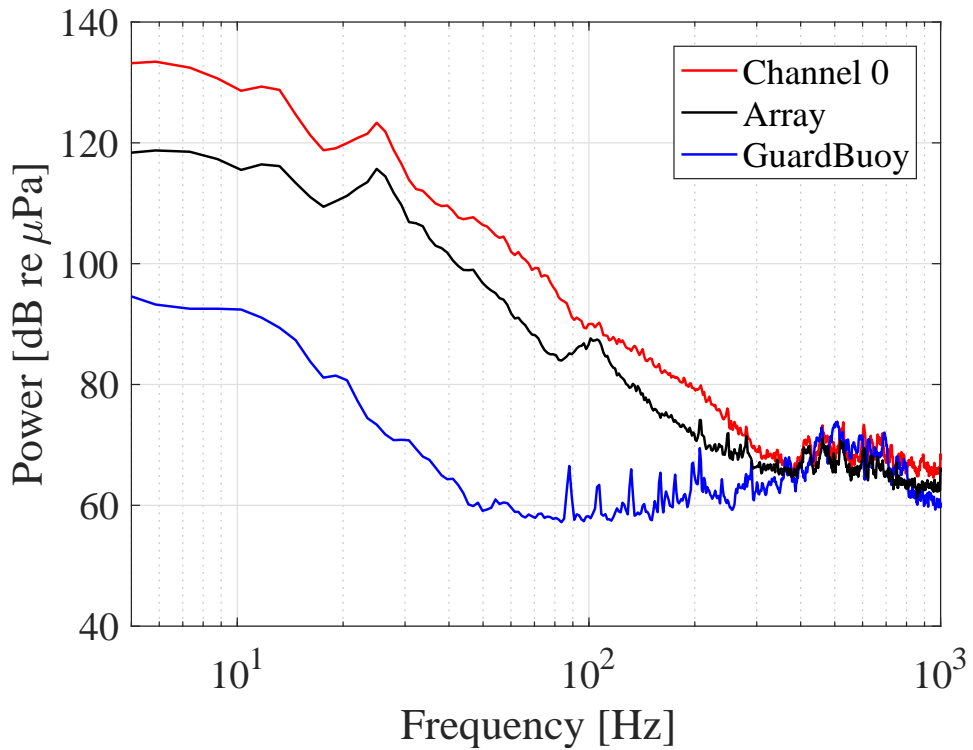


Fig. 8. Comparison of fixed single hydrophone (red), coherent array (black), and GuardBuoy (blue) signal power spectra at 1.5 hr into the deployment. The reduced levels and spectral critical frequency of the coherent array output relative to the fixed single hydrophone indicates effective flow noise suppression.

262 between the array and the GuardBuoy, as they are vertically and horizontally displaced relative to each
263 other.

264

V. DISCUSSION

265 *A. Spectral Critical Frequency*

266 Results show that critical frequency and flow speed are positively related, giving the intuitive result
267 that flow noise is prevalent in fast current conditions. The spectral critical frequency presents a method
268 of identifying flow noise prevalence within a signal.

269 The spectral critical frequency marks where ambient noise and flow noise have equal power, and
270 provides two important insights. Firstly, frequencies above the spectral critical frequency will contain a
271 mixture of ambient noise and flow noise. Secondly, frequencies below the spectral critical frequency will
272 be dominated by flow noise, since measurements in these frequencies contain spectral slopes that align
273 with turbulence theory. These insights are important, as they provide useful context for future signal level
274 and sound-source evaluations in tidal channel measurements.

275 *B. Spatial Coherence*

276 Spatial coherence results for different sensor combinations show that there are two distinct coherence
277 regions across the array: an incoherent flow noise region and a coherent ambient noise region. The
278 prevalence of these regions is quantified with the coherence critical frequency. Iterative calculations of the
279 coherence critical frequency were regressed against current speed. There is a positive relationship between
280 coherence critical frequency and current speed. The coherence critical frequency marks the frequency above
281 which flow noise is absent.

282 The spectral critical frequency provides a lower boundary, below which ambient noise is negligible,
283 and the coherence critical frequency provides an upper boundary, above which flow noise is negligible.
284 Frequencies between these bounds contain a mixture of flow noise and ambient noise. This explains why
285 the coherence critical frequencies are noticeably higher than those of the spectral method. The application
286 of spectral and coherence critical frequencies provides insight on the relative extent of both ambient noise
287 and flow noise within a signal.

288 *C. Beamforming*

289 By effectively treating the array as one sensor or hydrophone, signal processing can address the pseudo-
290 sound within low frequency data. Coherent averaging suppresses flow noise and enhances the detection of
291 propagating ambient noise. The coherent averaging employs a broadside approach with no steering angle
292 (19).

293 The results of the spectral critical frequencies derived from the beamformed array are shown in
294 Fig. 7. Evidently, the coherent array contains lower levels and lower critical frequencies than the fixed
295 single hydrophone (Fig. 7; Fig. 8). This implies that the coherent array is less affected by flow noise, and
296 contains a greater extent of ambient noise.

297 VI. CONCLUSION

298 Flow noise appears as: $f^{-5/3}$ noise when wavelength \gg sensor size, and f^{-m} noise, where the sensor's
299 finite dimension reduces the flow noise. f^{-m} is related to the flow speed over the array. The spectral critical
300 frequency is used to identify where ambient noise is negligible and the coherence critical frequency is
301 used to identify where flow noise is negligible.

302 Coherent processing (beamforming) suppresses flow noise and yields a lower spectral critical frequency
 303 than that of a fixed single hydrophone. An increased number of hydrophones and array length could
 304 improve array performance, allowing passive acoustic monitoring at arbitrarily low frequencies.

305

REFERENCES

- 306 [1] R. Karsten, A. Swan, and J. Culina, "Assessment of arrays of in-stream tidal turbines in the Bay of Fundy," *Phil. Trans. R. Soc. A*,
 307 vol. 371, no. 1985, p. 20120189, 2013.
- 308 [2] R. Inger, M. J. Attrill, S. Bearhop, A. C. Broderick, W. James Grecian, D. J. Hodgson, C. Mills, E. Sheehan, S. C. Votier, M. J. Witt
 309 *et al.*, "Marine renewable energy: potential benefits to biodiversity? An urgent call for research," *Journal of Applied Ecology*, vol. 46,
 310 no. 6, pp. 1145–1153, 2009.
- 311 [3] M. J. Dadswell, "Occurrence and migration of fishes in Minas Passage and their potential for tidal turbine interaction," 2010.
- 312 [4] A. Redden and M. Stokesbury, "Acoustic tracking of fish movements in the Minas Passage and FORCE demonstration area: Pre-turbine
 313 baseline studies (2011-2013)."
- 314 [5] D. Wang, M. Atlar, and R. Sampson, "An experimental investigation on cavitation, noise, and slipstream characteristics of ocean stream
 315 turbines," *Proceedings of the Institution of Mechanical Engineers, Part A: Journal of Power and Energy*, vol. 221, no. 2, pp. 219–231,
 316 2007.
- 317 [6] A. Lombardi, "Soundscape characterization in Grand Passage, Nova Scotia, a planned in-stream tidal energy site," 2016.
- 318 [7] M. K. Pine, A. G. Jeffs, and C. A. Radford, "Turbine sound may influence the metamorphosis behaviour of estuarine crab megalopae,"
 319 *PLoS One*, vol. 7, no. 12, p. e51790, 2012.
- 320 [8] M. Halvorsen, T. Carlson, and A. Copping, "Effects of tidal turbine noise on fish," *PNNL Report-20787 for US Dept of Energy*, WA,
 321 DC: by Pacific Northwest National Laboratory, Sequim, WA, pp. 1–41, 2011.
- 322 [9] M. Lighthill, "The Bakerian lecture, 1961. Sound generated aerodynamically," in *Proceedings of the Royal Society of London A:
 323 Mathematical, Physical and Engineering Sciences*, vol. 267, no. 1329. The Royal Society, 1962, pp. 147–182.
- 324 [10] M. Strasberg, "Nonacoustic noise interference in measurements of infrasonic ambient noise," *The Journal of the Acoustical Society of
 325 America*, vol. 66, no. 5, pp. 1487–1493, 1979.
- 326 [11] M. Van Dyke, *An album of fluid motion*. Parabolic Press Stanford, 1982, vol. 176.
- 327 [12] V. O. Knudsen, R. Alford, and J. Emling, "Underwater ambient noise," *J. Mar. Res.*, vol. 7, pp. 410–429, 1948.
- 328 [13] C. Bassett, J. Thomson, P. H. Dahl, and B. Polagye, "Flow-noise and turbulence in two tidal channels," *The Journal of the Acoustical
 329 Society of America*, vol. 135, no. 4, pp. 1764–1774, 2014.
- 330 [14] D. R. Barclay and M. J. Buckingham, "Depth dependence of wind-driven, broadband ambient noise in the Philippine Sea," *The Journal
 331 of the Acoustical Society of America*, vol. 133, no. 1, pp. 62–71, 2013.
- 332 [15] F. Dupont, C. G. Hannah, and D. Greenberg, "Modelling the sea level of the upper Bay of Fundy," *Atmosphere-Ocean*, vol. 43, no. 1,
 333 pp. 33–47, 2005.
- 334 [16] N. D. Merchant, T. R. Barton, P. M. Thompson, E. Pirotta, D. T. Dakin, and J. Dorocicz, "Spectral probability density as a tool for
 335 ambient noise analysis," *The Journal of the Acoustical Society of America*, vol. 133, no. 4, pp. EL262–EL267, 2013.
- 336 [17] M. J. Buckingham, "On the two-point cross-correlation function of anisotropic, spatially homogeneous ambient noise in the ocean and
 337 its relationship to the Green's function," *The Journal of the Acoustical Society of America*, vol. 129, no. 6, pp. 3562–3576, 2011.
- 338 [18] B. F. Cron and C. H. Sherman, "Spatial-correlation functions for various noise models," *The Journal of the Acoustical Society of
 339 America*, vol. 34, no. 11, pp. 1732–1736, 1962.

- 340 [19] G. B. Deane, M. J. Buckingham, and C. T. Tindle, "Vertical coherence of ambient noise in shallow water overlying a fluid seabed,"
341 *The Journal of the Acoustical Society of America*, vol. 102, no. 6, pp. 3413–3424, 1997.
- 342 [20] H. Cox, "Line array performance when the signal coherence is spatially dependent," *The Journal of the Acoustical Society of America*,
343 vol. 54, no. 6, pp. 1743–1746, 1973.

344 **Matthew Auvinen** Biography text here.

PLACE
PHOTO
HERE

345

346 **David Barclay** Biography text here.

PLACE
PHOTO
HERE

347